Energy &
Environment Nexus

Original Research

Open Access

https://doi.org/10.48130/een-0025-0004

# Molten salt regeneration of single-crystal $LiNi_{0.8}Co_{0.1}Mn_{0.1}O_2$ from end-of-life cathodes

Fangshu He[1#], Yuelin Lv[2#], Jingyuan Wu[1], Qi Zhang[1], Shuaipeng Hao[2], Lixia Yuan[2], Haiping Yang[1] and Yang Yang[1*]

Received: 17 June 2025

Revised: 14 July 2025

Accepted: 12 August 2025

Published online: 16 October 2025

## Abstract

High-nickel layered oxide cathode materials are widely used in power batteries due to their high capacity and energy density. However, during long-term cycling, these materials suffer from irreversible degradation, lithium loss and the formation of a rock salt phase, which limits their lifespan and recycling value. Traditional recycling methods, such as hydrometallurgy, can recover metal elements but fail to preserve the original structure of the material. This study proposes a direct regeneration strategy using a LiOH-$LiNiO_3$-lithium salicylate (LSA) ternary eutectic salt system to restore the structure and performance of spent $LiNi_{0.8}Co_{0.1}Mn_{0.1}O_2$ (NCM811) cathodes. This strategy leverages the efficient lithium-ion migration in the eutectic salt and the synergistic effect of LSA to achieve lithium compensation, lattice reconstruction and morphology regulation. XRD, SEM, Raman and XPS analyses showed that the regenerated R-NCM811 material eliminates the surface rock salt phase, reduces $Li^+/Ni^{2+}$ mixing and restores crystal integrity. Electrochemical tests revealed an initial discharge capacity of 196.0 mAh·$g^{-1}$ at 0.1 C, with a capacity retention of 76.0% after 200 cycles, outperforming most existing regeneration methods. This work provides a feasible path for the green regeneration of high-nickel ternary materials and supports the development of closed-loop recycling for high-performance batteries.

**Keywords:** High-nickel cathode, NCM811, Molten salt regeneration, Lithium compensation, Battery recycling

## Highlights

- A novel molten salt system enabled direct regeneration of degraded NCM811 cathodes.
- The eutectic salt removed surface rock salt phase and restores crystal ordering.
- Regenerated NCM811 delivered 196.0 mAh·$g^{-1}$ with 76.0% capacity retention after 200 cycles.
- The strategy addressed lithium loss and structural degradation in high-nickel cathodes.
- This work promotes scalable and eco-friendly recycling of lithium-ion batteries.

Authors contributed equally: Fangshu He and Yuelin Lv

* Correspondence: Yang Yang (y.yang100@outlook.com)

Full list of author information is available at the end of the article.

## Graphical abstract

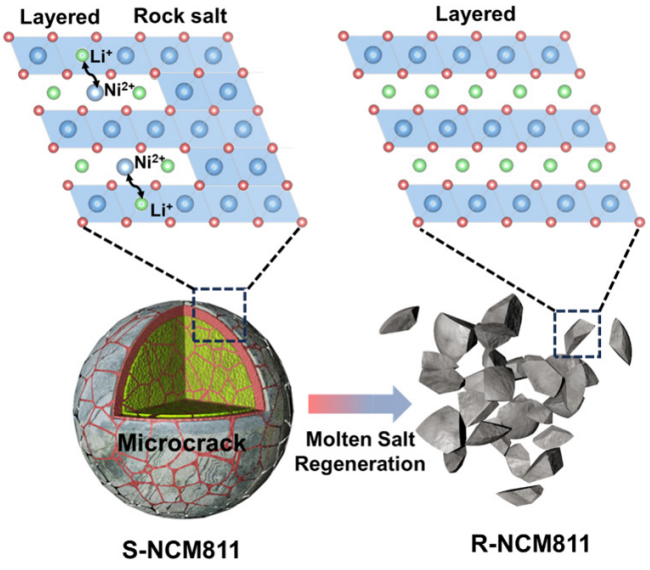


## Introduction

With the increasing demand for energy storage and the widespread adoption of electric vehicles, lithium-ion batteries (LIBs) have become the dominant technology for their high energy density, long lifespan and low self-discharge rates[1–3]. However, these batteries only have an average lifespan of 5–8 years. By 2030, the global stock of retired batteries is expected to exceed ten million tons[4–7], posing significant challenges in terms of resource management and environmental sustainability. Retired batteries contain valuable metals such as nickel (Ni), cobalt (Co) and lithium (Li), as well as reusable cathode materials, making them essential for resource recovery efforts[8–10].

Recycling methods for spent LIBs generally fall into three categories: pyrometallurgy, hydrometallurgy, and direct regeneration[11,12]. Although pyrometallurgical and hydrometallurgical methods are commercially established[13,14], they are associated with high energy consumption, environmental pollution and low economic value, as the products require further processing before being reused in new batteries[15,16]. In contrast, direct regeneration restores the performance of cathode materials by compensating for lithium loss, removing impurities, and repairing the structure[17]. This method, which preserves the original crystalline framework, offers significant advantages in terms of low energy consumption, short processing times and high economic efficiency, making it an ideal solution for the closed-loop utilization of high-nickel materials[18].

Previous studies have employed inorganic lithium salts such as LiOH combined with hydrothermal treatment or high-temperature sintering to regenerate high-nickel materials[19–21], which has led to some improvements in capacity and cycling stability. However, significant technical challenges remain, including: (1) uneven or insufficient lithium compensation, which fails to fully repair lithium loss and $Li^+/Ni^{2+}$ mixing during cycling, resulting in irreversible structural collapse[22]; (2) the difficulty of completely removing surface rock salt/spinel phases, with low efficiency in repairing microcracks, which affects long-term cycling stability[23,24]; (3) limited control over particle size and morphology via conventional lithium compensation, leading to stress concentration and structural degradation during subsequent charge/discharge cycles[25,26]. To address these issues, researchers explored the use of eutectic salt systems to enhance the interface wettability and $Li^+$ transfer efficiency that are often problematic in traditional lithium salt regeneration[14,27].

Organic lithium ligands, with their low decomposition temperature and good diffusion properties, have shown promise in assisting lattice repair and controlling valence state evolution at medium to low temperatures. This approach has demonstrated potential for improving the uniformity of structural reconstruction and controllability of morphology[28]. Recent studies have increasingly focused on using eutectic salt systems in direct regeneration processes, offering significant advantages due to their low melting points, high wettability, and enhanced ion diffusion properties. Binary eutectic molten salts, such as LiOH-$LiNO_3$[14] and LiOH-$Li_2CO_3$[22], have demonstrated the potential to recover the spent NCM cathodes. However, current research predominantly focuses on medium- to low-nickel systems (e.g., NCM523, NCM622), with limited exploration of high-nickel NCM811 due to its greater challenges. NCM811 exhibits severe structural collapse, significant lithium loss, and cation mixing during cycling, making it more thermally unstable and harder to regenerate compared to lower-nickel materials. Lithium salicylate (LSA) has been previously reported as a component in molten salt regeneration systems[25]. Compared with conventional binary molten salts such as LiOH-$Li_2CO_3$, LSA can more effectively lower the melting point, significantly improve molten salt fluidity and solid-liquid contact, thereby accelerating $Li^+$ diffusion within the bulk and enhancing the overall lithiation kinetics.

In this study, a direct regeneration strategy utilizing a LiOH-$LiNiO_3$-lithium salicylate (LSA) eutectic salt system was applied to restore lithium content and repair the structure of spent NCM811. The eutectic salt system, characterized by its low melting point, high wettability, and ability to control preferred crystal plane growth, facilitated the transformation of the regenerated NCM811 into a uniform single crystal. Multiple characterization techniques, including XRD Rietveld refinement, SEM, HRTEM, Raman spectroscopy, and XPS, confirmed that the regenerated NCM811 effectively eliminated the surface NiO rock salt phase and reduced the $Li^+/Ni^{2+}$ mixing in the bulk phase, resulting in a highly ordered layered structure. As a result, the regenerated sample exhibited an initial discharge capacity of 196.0 mAh·$g^{-1}$ at 0.1 C, and after 200 cycles, the capacity retention reached 76.0%. This work addresses core

issues such as structural collapse, lithium loss, and interface instability that commonly occur in spent high-nickel cathodes. Moreover, it proposes and validates a fast, uniform, and efficient regeneration route that overcomes the key technical gaps in lithium source uniformity and structural repair efficiency, providing new solutions and theoretical support for the closed-loop recycling of high-nickel materials.

# Experimental section

## Material pre-treatment

The spent NCM811 pouch cells were first fully discharged in NaCl aqueous solution. The cells were then disassembled in a fume hood, and the cathode electrodes were manually separated. Next, the electrode was flushed several times with anhydrous dimethyl carbonate (DMC) to remove residual electrolyte. The conductive agents and binders were not removed, and the materials were directly subjected to subsequent treatment. The cathode electrodes were then shredded and subjected to high-temperature calcination (500 °C, 3 h) to remove the PVDF binder and carbon materials. The resulting black powder was the pretreated degraded NCM811 (S-NCM811) material.

## Organic lithium salt-assisted regeneration

The degraded high-nickel ternary material, S-NCM811, was pre-treated and then mixed with a pre-prepared organic eutectic salt system to restore its crystal structure and composition. The eutectic system consists of inorganic lithium salts, LiOH and $LiNO_3$, in a molar ratio of 4:6. An equimolar amount of organic lithium salt, lithium salicylate (LSA), was added to form a ternary eutectic mixture (LiOH : $LiNO_3$ : LSA = 1.8:2.7:5.5). This mixture is solid at room temperature but melts upon heating, forming a homogeneous ionic liquid that facilitates the uniform distribution and migration of lithium ions. The ternary eutectic salt was mixed with S-NCM811 at a 1:2 molar ratio and thoroughly ground. The mixture was then calcined with a heating rate of 5 °C·min$^{-1}$ to reach 450 °C, where it was held for 3 h to promote the insertion of lithium. Afterward, the material was cooled naturally inside the furnace. The calcined product was subsequently mixed with an excess of 5 mol% LiOH to compensate for lithium loss during the high-temperature process. After further grinding, the sintering process was carried out with a heating rate of 5 °C·min$^{-1}$ to reach 750 °C, followed by a cooling rate of 10 °C·min$^{-1}$ until room temperature was achieved. The resulting powder, R-NCM811, was used for subsequent characterization and electrochemical performance evaluation.

## Material characterization methods

The crystal structure of the samples was characterized using an Empyrean X-ray diffraction (XRD) instrument (PANalytical B.V., Netherlands) with Cu K$\alpha$ radiation ($\lambda$ = 1.5406 Å). XRD measurements were performed over a 2$\theta$ range of 10° to 80° with a step size of 0.02°. The Rietveld refinement of the XRD patterns was carried out using the GSAS II software to obtain lattice parameters and phase composition information. The surface morphology of the samples was analyzed using a Sirion 200 Field Emission Scanning Electron Microscope (FESEM-1) (FEI, Netherlands) with a resolution of 1.5 nm at 10 kV. The microstructure and crystal orientation of the materials were examined using a high-resolution transmission electron microscope (HRTEM, FEI Tecnai G2 F20) with an operating voltage of 200 kV. Fast Fourier transform (FFT) analysis was also performed to assist in structural analysis. Raman spectroscopy was performed using a LabRAM HR800 spectrometer (Horiba Jobin Yvon, France) with a laser excitation wavelength of 532 nm. Each sample was scanned within a range of 100–3,000 cm$^{-1}$ for 10 s. X-ray photoelectron spectroscopy (XPS) was conducted using a Thermo Scientific K-Alpha instrument with a monochromatic Al K$\alpha$ source (E = 1,486.68 eV). The operating conditions included a voltage of 12.0 kV, a current of 0.006 A, and a vacuum pressure lower than $10^{-9}$ mbar.

## Electrochemical performance testing

For electrochemical performance testing, CR2032 coin cells were assembled with lithium foil as the anode electrode and a 1 M $LiPF_6$ solution in a mixture of EC : DEC : DMC (1:1:1 volume ratio) as the electrolyte. The active material, Super P, and PVDF were mixed in a mass ratio of 8:1:1 and coated onto aluminum foil to form the cathode. Charge–discharge tests were performed using Neware and Land battery testing systems within a voltage range of 3.0 to 4.3 V. Cyclic voltammetry (CV) and electrochemical impedance spectroscopy (EIS) were carried out using a Princeton Electrochemical Workstation.

# Results and discussion

## Morphological and structural characterization

To further elucidate the structural evolution of S-NCM811 during degradation and regeneration, XRD analyses of S-NCM811 and regenerated R-NCM811 samples were performed, as shown in Fig. 1a. Both materials exhibit the typical characteristics of the R-3m space group, consistent with the $\alpha$-$NaFeO_2$ layered structure[29]. R-NCM811 displayed clear diffraction peaks at the (003), (101), and (104) planes, indicating a well-ordered crystal structure. In contrast, S-NCM811 showed weaker and broadened diffraction peaks, along with the presence of a NiO impurity phase (JCPDS 44-1159), reflecting significant structural degradation[5].

ICP-OES was employed to assess the elemental composition of both S-NCM811 and R-NCM811. The results, as presented in Supplementary Tables S1 and S2, showed the elemental contents of Li, Ni, Co, and manganese (Mn) in both materials, as well as the molar ratio of Li to Ni. Notably, S-NCM811 exhibited a molar ratio of Li/(Ni + Co + Mn) of 0.73, indicating a substantial loss of lithium, which contributes to the observed structural degradation. In comparison, R-NCM811 showed a higher Li/(Ni + Co + Mn) ratio of 1.03, indicating effective lithium compensation during the regeneration process and an improved structural integrity. This is consistent with the XRD results, where R-NCM811 demonstrated a restored, well-ordered layered structure after regeneration. The magnified views in Fig. 1b and c revealed that the (003) peak of S-NCM811 shifted to a lower angle, indicating an expansion along the c-axis. This is mainly attributed to lithium loss, which increases electrostatic repulsion between the transition metal layers[30]. Conversely, the (003) peak of R-NCM811 shifted back to a higher angle, signifying a recovery of the interlayer spacing and the restoration of structural order. Furthermore, the intensity ratio of $I_{(003)}/I_{(104)}$ for S-NCM811 decreased to 1.00, suggesting a high degree of $Li^+/Ni^{2+}$ mixing[26,31]. However, the $I_{(003)}/I_{(104)}$ ratio for R-NCM811 was 1.11, indicating a well-ordered layered structure. Additionally, the (108) and (110) peaks in S-NCM811 exhibited noticeable peak splitting, indicative of a collapsed layered structure, while R-NCM811 showed clear peak splitting, confirming the successful restoration of the layered order.

SEM observations were conducted on both S-NCM811 and R-NCM811 samples. As shown in Fig. 1d, the surface of S-NCM811 particles was rough, exhibiting significant fragmentation and microcracks, which resulted from lattice distortion and volume changes after cycling. These cracks provided pathways for electrolyte penetration, accelerating side reactions and further weakening the structural integrity of the electrode. Additionally, residual polyvinylidene fluoride (PVDF) binder and carbon black conductive additives were visible on the particle surfaces. In contrast, the regenerated

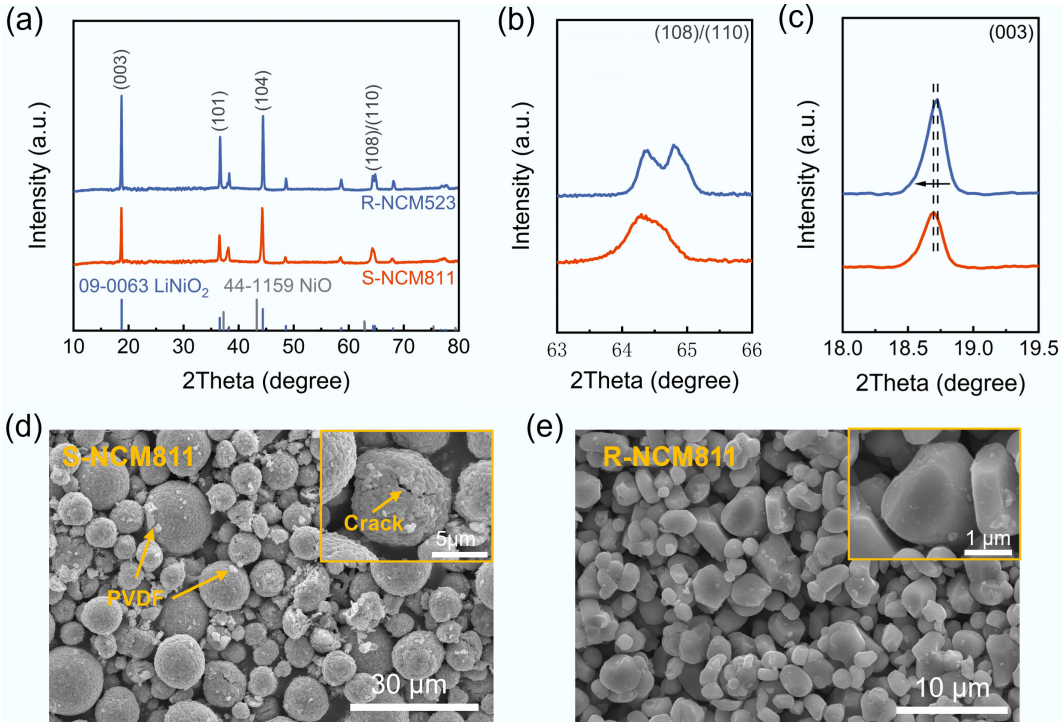


**Fig. 1** (**a**) XRD patterns and magnified XRD patterns of (**b**) (108)/(110) peaks, and (**c**) (003) peak for S-NCM811 and R-NCM811; (**d**), (**e**) SEM images for S-NCM811 and R-NCM811.

R-NCM811 sample (Fig. 1e) exhibited markedly different morphological features. The particle surfaces were smoother, with well-defined boundaries and a more uniform particle size distribution, suggesting that the material underwent thorough ion exchange and phase reconstruction during the regeneration process. The high-temperature sintering process effectively removed surface impurities and promoted recrystallization, healing the microcracks. Furthermore, some R-NCM811 particles displayed a single-crystal morphology, indicating that this regeneration strategy can partially transform fragmented polycrystalline material into an ordered structure.

To further investigate the microstructure of the regenerated sample, HRTEM analyses were performed, as shown in Fig. 2a. In the original S-NCM811 sample, images extending from the bulk (Region II) to the outer surface (Region I) revealed the formation of a rock-salt phase structure on the surface, corresponding to the (111) and (220) planes in the FFT image. This transformation from a layered to a rock salt structure is primarily due to lithium loss and $Li^+/Ni^{2+}$ mixing[24,32], which corresponds to the ICP-OES results (Supplementary Table S1), inducing charge imbalance and is the core reason for the degradation of its electrochemical performance. Despite the surface structural transition, the internal structure of S-NCM811 still retained a layered arrangement, with the (104) crystal plane interlayer spacing of 0.241 nm (Region II), indicating that the structure could theoretically be restored to its original state through lithium supplementation.

The regenerated R-NCM811 sample, on the other hand, showed significant structural recovery. As shown in Fig. 2b, from the outer surface to the internal regions, a highly ordered layered structure was present. Notably, in Region III, clear lattice fringes corresponding to the (003) plane were observed, with an interlayer spacing of 0.476 nm; similarly, in Region IV, the lattice fringes were evenly arranged, with an interlayer spacing of 0.481 nm. This indicates that the crystal structure was restored to a highly ordered layered phase from the surface to the interior. FFT images of both regions further confirmed the continuity and integrity of the crystal orientation. This strategy effectively facilitates reconstruction of the rock-salt phase to the complete layered phase, providing a solid structural foundation for the subsequent excellent electrochemical performance.

## Electrochemical performance

This study compares the performance differences of NCM811 materials before and after regeneration. As shown in Fig. 3a, the initial discharge capacity of S-NCM811 was only 105.7 $mAh{\cdot}g^{-1}$, which is attributed to the rock salt phase on the surface, $Li^+/Ni^{2+}$ mixing, and lithium loss. In contrast, after regeneration, R-NCM811 showed a significant recovery with an initial capacity of 196.0 $mAh{\cdot}g^{-1}$, indicating effective lithium compensation and lattice structure reconstruction. Figure 3b presents the cycling performance of both materials within the voltage range of 3.0–4.3 V at 1 C. The discharge capacity of S-NCM811 was only 18.1 $mAh{\cdot}g^{-1}$, while R-NCM811 achieved a discharge capacity of 175.4 $mAh{\cdot}g^{-1}$. After 200 cycles, R-NCM811 retained a capacity of 133.3 $mAh{\cdot}g^{-1}$, resulting in a capacity retention of 76.0%. This demonstrates a significant improvement in the structural stability of the regenerated material.

The rate performance test shown in Fig. 3c indicates that R-NCM811 outperforms S-NCM811 at all rates from 0.1 to 5 C, with especially good performance at higher rates. This suggests that the $Li^+$ diffusion kinetics and electron transport pathways of the regenerated electrode have been effectively restored. To investigate the redox behavior and electrochemical reversibility, cyclic voltammetry (CV) tests were performed. S-NCM811 did not exhibit clear oxidation/reduction peaks at 0.1 $mV{\cdot}s^{-1}$(Fig. 3d), reflecting its almost non-existent lithium storage capacity. In contrast, R-NCM811 (Fig. 3e) showed well-defined and symmetric redox peaks, with a small potential separation of only 0.023 V, compared to 0.184 V for

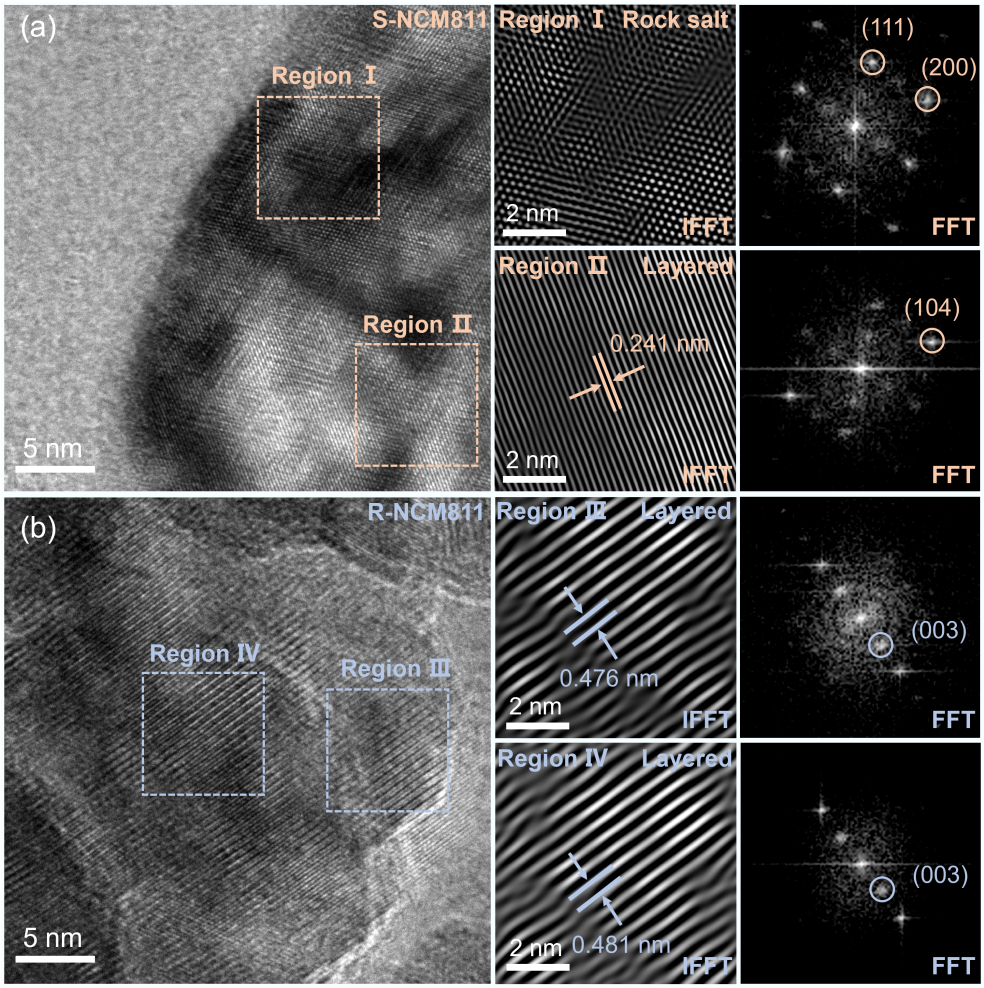


**Fig. 2** HRTEM images for (**a**) S-NCM811, and (**b**) R-NCM811.

S-NCM811, indicating significantly improved reversibility. The $Li^+$ diffusion kinetics of R-NCM811 were notably enhanced after regeneration. As shown in Fig. 3f and g, R-NCM811 still maintained good peak shapes at different scan rates of CV (0.1 $mV{\cdot}s^{-1}$ → 1.0 $mV{\cdot}s^{-1}$), suggesting superior ion migration and interface reaction kinetics. The peak current shows a linear relationship with the square root of the scan rate, with a higher slope indicating a faster $Li^+$ diffusion rate. The slope for R-NCM811 was 5.37, compared to 0.51 for S-NCM811 (Fig. 3h).

To gain insight into the regulation of interface reaction kinetics and electrode impedance behavior during the regeneration process, *in situ* electrochemical impedance spectroscopy (EIS) was conducted on S-NCM811 and R-NCM811 during their first charge-discharge cycle. The specific voltage points for testing are shown in Fig. 3i. The Nyquist plots, presented in Fig. 3j, consist of a high-frequency semicircle and a low-frequency sloping line[33,34]. By fitting the EIS data with an equivalent circuit (see Supplementary Tables S3 and S4), the evolution of the interfacial film resistance ($R_f$) and charge transfer resistance ($R_{ct}$) at various voltage points was obtained, as shown in Fig. 3k. It is evident from Fig. 3j that R-NCM811 exhibited smaller semicircle diameters and lower overall impedance throughout the charge–discharge process, indicating superior interfacial reaction kinetics. Fig. 3k further quantifies the changes in $R_{ct}$ and $R_f$ at each voltage point for different samples. The $R_{ct}$ and $R_f$ of S-NCM811 varied greatly at different voltages, which indicates the presence of obvious side reactions or structural instability at the interface. Alternatively, R-NCM811 exhibited consistently lower $R_{ct}$ and $R_f$ across the entire voltage range, with a smaller variation, indicating a more stable interface structure and lower energy barriers for $Li^+$ migration. This disparity can be primarily attributed to the restoration of lattice order, and the elimination of the interfacial rock-salt phase during the regeneration process.

## Repair mechanism analysis

To elucidate the structural repair mechanism of nickel-rich cathode materials during the organic eutectic salt-assisted regeneration process, a systematic analysis was performed using XRD Rietveld refinement, Raman spectroscopy, and XPS. This analysis revealed the synergistic evolution of crystal structure ordering and oxidation states of transition metals. As shown in Fig. 4a and b, the Rietveld refinement results revealed that S-NCM811 exhibited significant structural disorder after prolonged cycling, characterized by approximately 5.1% NiO rock salt phase and the $Li^+/Ni^{2+}$ mixing reaching 6.5%. Furthermore, the c parameter of the spent material was 14.2471 Å, higher than the regenerated material at 14.2066 Å (Supplementary Tables S5 and S6), a change primarily attributed to lithium loss, which increased electrostatic repulsion between the transition metal layers. Whereas, R-NCM811 showed complete elimination of the NiO rock salt phase, and the $Li^+/Ni^{2+}$ mixing was reduced to 3.3%. These results suggest that the organic eutectic lithium salt system, by releasing oxidative species, facilitates the reoxidation of $Ni^{2+}$, effectively reversing the material from the rock-salt phase to an ordered layered structure.

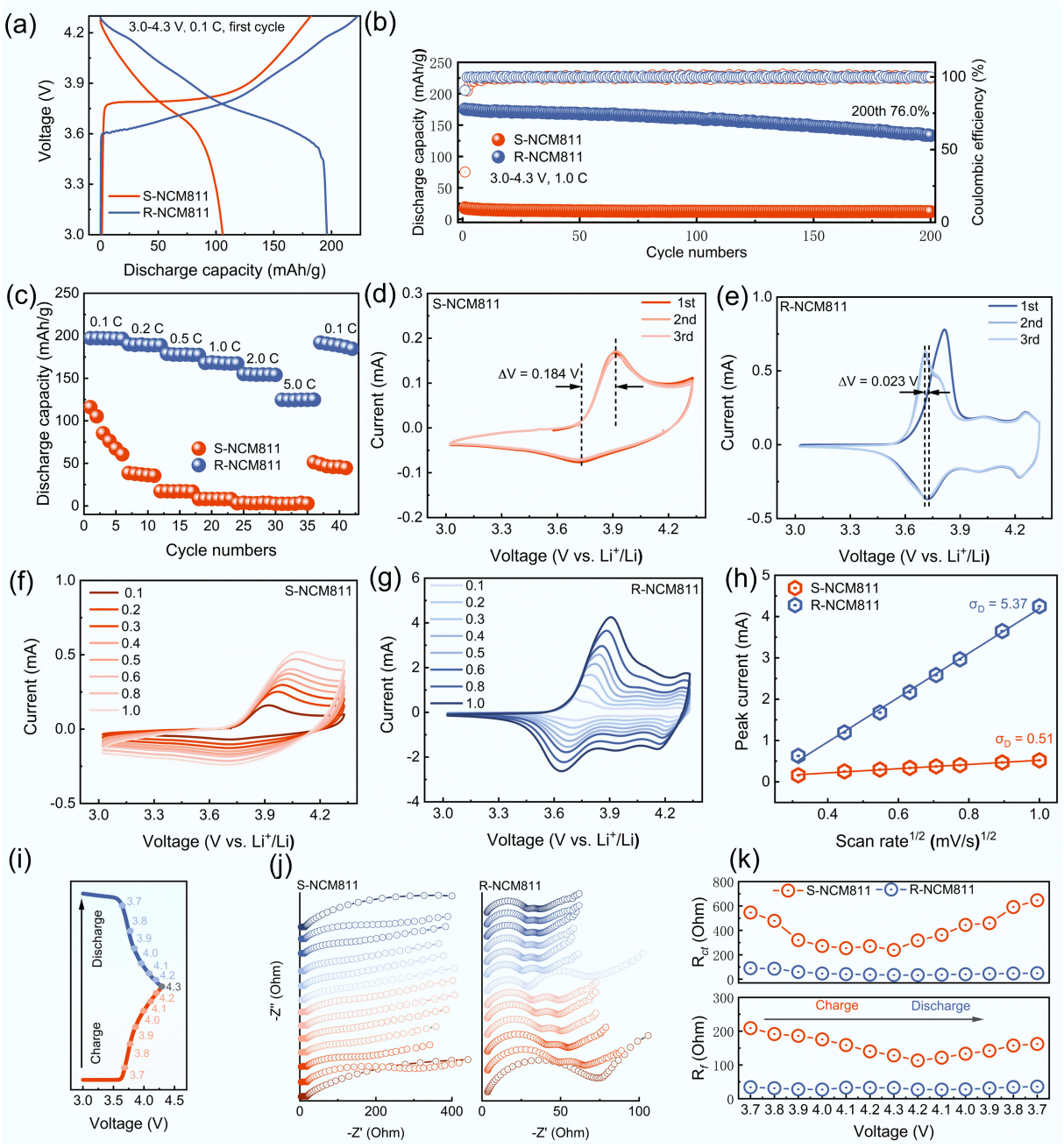


**Fig. 3** Electrochemical performance of S-NCM811 and R-NCM811: (**a**) Charge and discharge curves at 0.1 C. (**b**) Cycling performance. (**c**) Rate performance. (**d**), (**e**) CV curves at 0.1 mV·s$^{-1}$. (**f**), (**g**) CV curves at different scan rates. (**h**) Linear fitting curves with various sweep speeds vs peak current. (**i**) Voltage profiles during in situ EIS measurement. (**j**), (**k**) *In-situ* Nyquist curves and resistance values for S-NCM811 and R-NCM811.

As shown in Fig. 4c, the Raman spectrum of S-NCM811 exhibited only the $A_1g$ vibration peak, which corresponded to the characteristic peak of NiO, indicating that the surface structure has deteriorated from a layered to a rock-salt phase[35]. In contrast, R-NCM811 displayed both $A_{1g}$ and $E_g$ peaks, matching the characteristic peaks of layered $LiNiO_2$, indicating the removal of the surface NiO[36], in agreement with the XRD refinement results.

This structural restoration was strongly related to the synergistic effect of LSA in the eutectic system. LSA lowered the melting point, thereby improving molten salt flow and solid-liquid contact, which enhanced $Li^+$ transport into the bulk. In parallel, the decomposition of LSA at high temperatures produced organic oxidizing species such as nitrobenzene, promoting the oxidation of $Ni^{2+}$ to $Ni^{3+}$ and suppressing the formation of the NiO rock salt phase[25]. This dual function enables more complete phase reconstruction, accounting for the improved layered features observed in both XRD and Raman analyses. These findings are consistent with similar findings reported for organic eutectic salt-assisted regeneration of Ni-rich cathodes[14].

As seen in Fig. 4d, XPS results further verified these observations. The Ni 2p peak of S-NCM811 shifted to a lower binding energy compared to R-NCM811, suggesting a lower oxidation state of Ni. Further analysis showed that the proportion of $Ni^{2+}$ in S-NCM811 was as high as 51.5%, which is prone to $Li^+/Ni^{2+}$ mixing. This is due to the similar radii of $Li^+$ and $Ni^{2+}$ (0.76 Å and 0.69 Å, respectively) and the presence of a large number of lithium vacancies, which

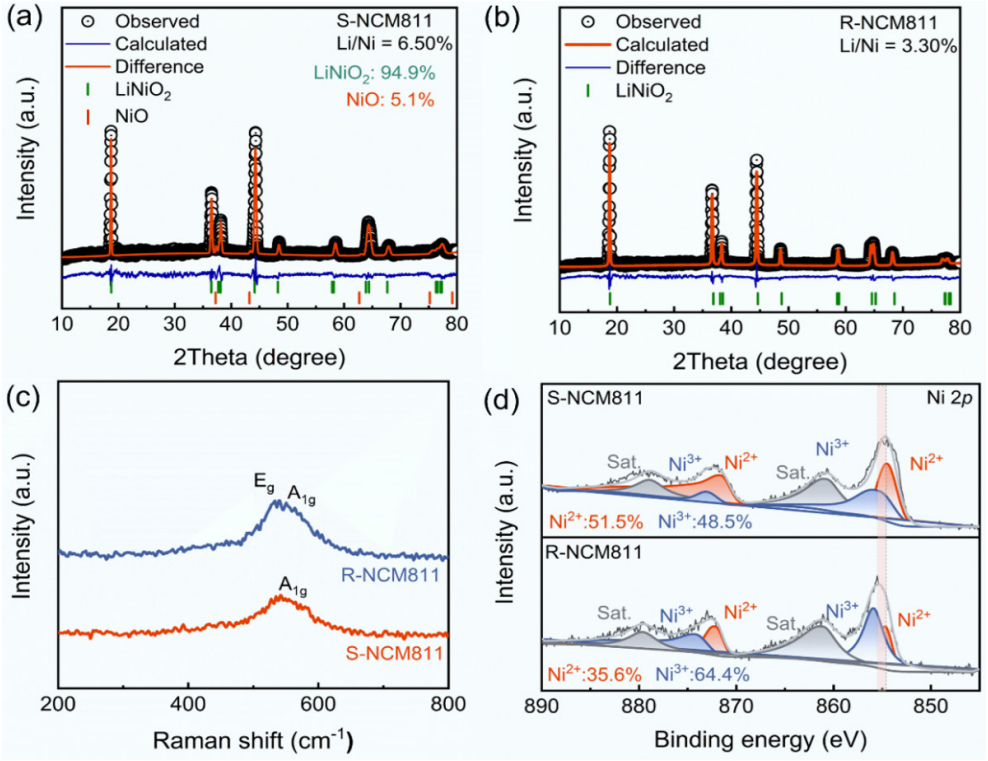


**Fig. 4** (**a**), (**b**) XRD Rietveld refinement patterns of S-NCM811 and R-NCM811. (**c**) Raman spectra of S-NCM811 and R-NCM811. (**d**) Ni 2p XPS spectra of S-NCM811 and R-NCM811.

reduces the diffusion energy barrier of $Ni^{2+}$ into the lithium layer[37]. In R-NCM811, however, the proportion of $Ni^{2+}$ decreased to 35.6%. This oxidation state transition during the regeneration process facilitates the reoxidation of $Ni^{2+}$ to $Ni^{3+}$, thereby accelerating the re-insertion of lithium.

## Conclusions

A novel direct regeneration strategy using a LiOH-$LiNiO_3$-lithium salicylate eutectic salt system has been successfully employed for high-nickel NCM811 cathode materials. This method utilizes the synergistic effect of eutectic salts, which not only compensates for lithium loss but also enables the structural reconstruction of the material. By using this strategy, the crystalline structure of the NCM811 cathode is restored, the $Li^+/Ni^{2+}$ mixing is reduced, and the detrimental surface NiO rock salt phase is fully eliminated. Characterization techniques, including XRD, SEM, HRTEM, Raman, and XPS, confirmed the success of this regeneration process, leading to a highly ordered layered structure in the regenerated R-NCM811. The electrochemical performance of the regenerated material demonstrated substantial improvements. The initial discharge capacity of R-NCM811 reached 196.0 mAh·$g^{-1}$, significantly higher than the degraded S-NCM811, which only exhibited 105.7 mAh·$g^{-1}$. Furthermore, after 200 cycles, the R-NCM811 maintained 76.0% of its capacity, indicating excellent cycling and structural stability. This work provides a novel approach for the development of direct regeneration of cathode materials for lithium-ion batteries.

Although this regeneration strategy effectively restored spent NCM811 cathodes, it was only demonstrated at the lab scale. To enable industrial scale-up, further optimization of $Li^+$ compensation and reaction kinetics is required. Additionally, future work will focus on conducting a comprehensive LCA to evaluate the environmental sustainability of the method.

## Supplementary information

It accompanies this paper at: https://doi.org/10.48130/een-0025-0004.

## Author contributions

All authors contributed to the work presented in this paper. FH and YL designed the research and performed the experiments. SH conducted the material characterization and data analysis. LY and HY provided guidance throughout the experiments and contributed to the data interpretation. FH, YL, and YY co-wrote the paper. All authors participated in the manuscript discussion and review.

## Data availability

The data supporting the present work can be found in the Supplementary information.

## Acknowledgments

The authors acknowledge the State Key Laboratory of Materials Processing and Die & Mould Technology of Huazhong University of Science and Technology for SEM measurements, and the Analytical and Testing Center of Huazhong University of Science and Technology for XRD measurements.

## Funding

The authors acknowledge research project 52576210 supported by National Natural Science Foundation of China.

## Declarations

### Competing interests

The authors declare that they have no conflict of interest.

## Author details

[1]State Key Laboratory of Coal Combustion, Huazhong University of Science and Technology, Wuhan, Hubei 430074, China; [2]State Key Laboratory of Material Processing and Die & Mould Technology, School of Materials Science and Engineering, Huazhong University of Science and Technology, Wuhan, Hubei 430074, China

## References

[1] Bauer C, Burkhardt S, Dasgupta NP, Ellingsen LAW, Gaines LL, et al. 2022. Charging sustainable batteries. *Nature Sustainability* 5:176–178

[2] Fan E, Li L, Wang Z, Lin J, Huang Y, et al. 2020. Sustainable recycling technology for Li-Ion batteries and beyond: challenges and future prospects. *Chemical Reviews* 120:7020–7063

[3] Fan M, Chang X, Guo YJ, Chen WP, Yin YX, et al. 2021. Increased residual lithium compounds guided design for green recycling of spent lithium-ion cathodes. *Energy & Environmental Science* 14:1461–1468

[4] Fan M, Meng Q, Chang X, Gu CF, Meng XH, et al. 2022. *In situ* electrochemical regeneration of degraded $LiFePO_4$ electrode with functionalized prelithiation separator. *Advanced Energy Materials* 12:2103630

[5] Ji G, Wang J, Liang Z, Jia K, Ma J, et al. 2023. Direct regeneration of degraded lithium-ion battery cathodes with a multifunctional organic lithium salt. *Nature Communications* 14:584

[6] Mao J, Ye C, Zhang S, Xie F, Zeng R, et al. 2022. Toward practical lithium-ion battery recycling: adding value, tackling circularity and recycling-oriented design. *Energy & Environmental Science* 15:2732–2752

[7] Zhang R, Hanaoka T. 2021. Deployment of electric vehicles in China to meet the carbon neutral target by 2060: Provincial disparities in energy systems, $CO_2$ emissions, and cost effectiveness. *Resources, Conservation and Recycling* 170:105622

[8] Mrozik W, Ali Rajaeifar M, Heidrich O, Christensen P. 2021. Environmental impacts, pollution sources and pathways of spent lithium-ion batteries. *Energy & Environmental Science* 14:6099–6121

[9] Raj B, Sahoo MK, Nikoloski A, Singh P, Basu S, et al. 2023. Retrieving Spent Cathodes from Lithium-Ion Batteries through Flourishing Technologies. *Batteries & Supercaps* 6

[10] Xu P, Tan DHS, Jiao B, Gao H, Yu X, et al. 2023. A materials perspective on direct recycling of lithium-ion batteries: principles, challenges and opportunities. *Advanced Functional Materials* 33:2213168

[11] Yao Q, Xiao F, Lin C, Xiong P, Lai W, et al. 2023. Regeneration of spent lithium manganate into cation-doped and oxygen-deficient $MnO_2$ cathodes toward ultralong lifespan and wide-temperature-tolerant aqueous Zn-ion batteries. *Battery Energy* 2:20220065

[12] Yu J, Ma B, Qiu Z, Wang C, Chen Y. 2023. Separation and recovery of valuable metals from ammonia leaching solution of spent lithium-ion batteries. *ACS Sustainable Chemistry & Engineering* 11:9738–9750

[13] Liao H, Zhao S, Cai M, Dong Y, Huang F. 2023. Direct conversion of waste battery cathodes to high-volumetric-capacity anodes with assembled secondary-particle morphology. *Advanced Energy Materials* 13:2300596

[14] Shi Y, Zhang M, Meng YS, Chen Z. 2019. Ambient-pressure relithiation of degraded $Li_xNi_{0.5}Co_{0.2}Mn_{0.3}O_2$ ($0 < x < 1$) via eutectic solutions for direct regeneration of lithium-ion battery cathodes. *Advanced Energy Materials* 9:1900454

[15] Wang J, Li D, Zeng W, Chen X, Zhang Y, et al. 2025. Degradation mechanism, direct regeneration and upcycling of ternary cathode material for retired lithium-ion power batteries. *Journal of Energy Chemistry* 102:534–554

[16] Wang J, Ma J, Zhuang Z, Liang Z, Jia K, et al. 2024. Toward direct regeneration of spent lithium-ion batteries: a next-generation recycling method. *Chemical Reviews* 124:2839–2887

[17] Xu P, Yang Z, Yu X, Holoubek J, Gao H, et al. 2021. Design and optimization of the direct recycling of spent li-ion battery cathode materials. *ACS Sustainable Chemistry & Engineering* 9:4543–4553

[18] Zhu XH, Li YJ, Gong MQ, Mo R, Luo SY, et al. 2023. Recycling valuable metals from spent lithium-ion batteries using carbothermal shock method. *Angewandte Chemie International Edition* 62:e202300074

[19] Chen D, Mu S. 2024. Molten salt-assisted synthesis of catalysts for energy conversion. *Advanced Materials* 36:e2408285

[20] Deng B, Zhou Z, Wang W, Wang D. 2020. Direct recovery and efficient reutilization of degraded ternary cathode materials from spent lithium-ion batteries via a homogeneous thermochemical process. *ACS Sustainable Chemistry & Engineering* 8:14022–14029

[21] Hansen BB, Spittle S, Chen B, Poe D, Zhang Y, et al. 2021. Deep eutectic solvents: a review of fundamentals and applications. *Chemical Reviews* 121:1232–1285

[22] Jiang G, Zhang Y, Meng Q, Zhang Y, Dong P, et al. 2020. Direct regeneration of $LiNi_{0.5}Co_{0.2}Mn_{0.3}O_2$ cathode from spent lithium-ion batteries by the molten salts method. *ACS Sustainable Chemistry & Engineering* 8:18138–18147

[23] Liu X, Wang M, Deng L, Cheng YJ, Gao J, et al. 2022. Direct regeneration of spent lithium iron phosphate via a low-temperature molten salt process coupled with a reductive environment. *Industrial & Engineering Chemistry Research* 61:3831–3839

[24] Qin Z, Wen Z, Xu Y, Zheng Z, Bai M, et al. 2022. A ternary molten salt approach for direct regeneration of $LiNi_{0.5}Co_{0.2}Mn_{0.3}O_2$ cathode. *Small* 18:2106719

[25] Liu X, Wang R, Liu S, Pu J, Xie H, et al. 2023. Organic eutectic salts-assisted direct lithium regeneration for extremely low state of health Ni-rich cathodes. *Advanced Energy Materials* 13:2302987

[26] Ma J, Wang J, Jia K, Liang Z, Ji G, et al. 2022. Adaptable eutectic salt for the direct recycling of highly degraded layer cathodes. *Journal of the American Chemical Society* 144:20306–20314

[27] Smith EL, Abbott AP, Ryder KS. 2014. Deep Eutectic Solvents (DESs) and Their Applications. *Chemical Reviews* 114:11060–11082

[28] Wang T, Luo H, Bai Y, Li J, Belharouak I, et al. 2020. Direct recycling of spent NCM cathodes through ionothermal lithiation. *Advanced Energy Materials* 10:2001204

[29] Jeong M, Lee W, Yun S, Choi W, Park H, et al. 2022. Strategic approach to diversify design options for Li-Ion batteries by utilizing low-Ni layered cathode materials. *Advanced Energy Materials* 12:2103052

[30] Jia K, Yang G, He Y, Cao Z, Gao J, et al. 2024. Degradation mechanisms of electrodes promotes direct regeneration of spent li-ion batteries: a review. *Advanced Materials* 36:2313273

[31] Jung SK, Gwon H, Hong J, Park KY, Seo DH, et al. 2014. Understanding the degradation mechanisms of $LiNi_{0.5}Co_{0.2}Mn_{0.3}O_2$ cathode material in lithium ion batteries. *Advanced Energy Materials* 4:1300787

[32] Qin Z, Zhang Y, Luo W, Zhang T, Wang T, et al. 2023. A universal molten salt method for direct upcycling of spent Ni-rich cathode towards single-crystalline Li-rich cathode. *Angewandte Chemie International Edition* 62:e202218672

[33] Wang D, Xin C, Zhang M, Bai J, Zheng J, et al. 2019. Intrinsic role of cationic substitution in tuning Li/Ni mixing in high-Ni layered oxides. *Chemistry of Materials* 31:2731–2740

[34] Zhu H, Wang Z, Chen L, Hu Y, Jiang H, et al. 2023. Strain engineering of Ni-rich cathode enables exceptional cyclability in pouch-type full cells. *Advanced Materials* 35:2209357

[35] Hao S, Yang J, Li Y, Liu S, Jiang S, et al. 2025. Utilizing oxygen-vacancy-rich violet tungsten oxide enabling ultralong cycling of nickel-rich cathodes at high voltage. *ACS Nano* 19:7263–7272

[36] Hao S, Lv Y, Zhang Y, Liu S, Tan Z, et al. 2025. Restoration of $Li^+$ pathways in the [010] direction during direct regeneration for spent $LiFePO_4$. *Energy & Environmental Science* 18:3750–3760

[37] Hao S, Li Y, Yang J, Wang S, Tan Z, et al. 2023. External-to-internal synergistic strategy to enable multi-scale stabilization of $LiCoO_2$ at high-voltage. *Journal of Energy Chemistry* 76:516–527